

THESIS FOR THE DEGREE OF LICENTIATE OF  
ENGINEERING

Characterisation of terahertz integrated  
membrane circuits

JOHANNA HANNING

Department of Microtechnology and Nanoscience (MC2)  
CHALMERS UNIVERSITY OF TECHNOLOGY  
Gothenburg, Sweden, May 2015

Characterisation of terahertz integrated membrane circuits  
JOHANNA HANNING

© JOHANNA HANNING, 2015

ISSN 1652-0769

Technical Report MC2-299

Department of Microtechnology and Nanoscience (MC2)  
Terahertz and Millimetre Wave Laboratory  
Chalmers University of Technology  
SE-412 96 Gothenburg  
Sweden  
Phone: + 46 (0)31-772 1000

Cover:

Illustration of the TRL-kit presented in this thesis, with the adapter block connected to two VNA extender modules with two rectangular waveguides, and the interchangeable DUT block.

This report is written in L<sup>A</sup>T<sub>E</sub>X

Printed by TeknologTryck  
Gothenburg, Sweden, May 2015

For Eskil and Andreas





Characterisation of terahertz integrated membrane circuits

JOHANNA HANNING

Department of Microtechnology and Nanoscience (MC2)

Chalmers University of Technology

# Abstract

In this thesis a novel measurement setup and thru-reflect-line (TRL) calibration kit for vector network analyser (VNA) measurements at 220 GHz to 325 GHz (WR-03) is presented. Measurements on passive membrane circuit devices under test (DUTs) show improvement in the S-parameters compared to a waveguide integrated membrane circuit setup in previous work, especially in reducing the ripples and increasing repeatability of the measurements.

VNA measurements provide a challenge when measuring on waveguide integrated membrane circuit devices at terahertz frequencies. In this setup, phase uncertainty in the measurements, due to waveguide width tolerance, is reduced by shortening the access waveguides. Because both waveguide inputs are placed in the same flange, the access waveguides can be made much shorter. However, in order to accommodate different DUT and TRL line lengths, two bends were introduced in each waveguide, and the trade-off between sharper bends or longer access waveguides effect on uncertainty, investigated.

By the use of an adapter block, which puts the VNA extender outputs in the same flange, phase uncertainty due to cable flex is eliminated by locking the VNA frequency extenders in position during the entire measurement.

**Keywords:** THz, membrane circuit, TRL, calibration, VNA, 220–325 GHz, WR-03, single-flange 2-port, measurement uncertainty, S-parameter, cable flex, waveguide width error

# List of publications

## Appended papers

The following papers constitute the main work for this thesis:

- [A] **J. Hanning**, J. Stenarson, K. Yhland, P. J. Sobis, T. Bryllert, and J. Stake, “Single-flange 2-port TRL calibration for accurate THz S-parameter measurements of waveguide integrated circuits,” *IEEE Transactions on Terahertz Science and Technology*, September 2014, vol. 4, no. 5, pp. 582–587. <http://dx.doi.org/10.1109/TTHZ.2014.2342497>
  
- [B] **J. Hanning**, J. Stenarson, K. Yhland, P. J. Sobis, T. Bryllert, and J. Stake, “Single flange 2-port design for THz integrated circuit S-parameter characterization,” in *38th International Conference on Infrared, Millimeter and Terahertz Waves (IRMMW-THz)*, 2013. <http://dx.doi.org/10.1109/IRMMW-THz.2013.6665800>

## Other papers

The following papers are not included since the content is beyond the scope of this thesis:

- [a] K. Eriksson, P. J. Sobis, S. E. Gunnarsson, **J. Hanning**, and H. Zirath, “InP DHBT amplifier modules operating between 150–300 GHz using membrane technology,” *IEEE Transactions on Microwave Theory and Techniques*, vol. 63, no. 2, pp. 433–440, February 2015.
- [b] P. F. -X. Neumaier, H. Richter, J. Stake, H. Zhao, A. Y. Tang, V. Drakinskiy, P. Sobis, A. Emrich, A. Hülsmann, T. K. Johansen, T. Bryllert, **J. Hanning**, V. Krozer, and H. -W. Hübers, “Molecular Spectroscopy With a Compact 557-GHz Heterodyne Receiver” *IEEE Transactions on Terahertz Science and Technology*, vol. 4, no. 4, pp. 469–478, July 2014.
- [c] J. Vukusic, T. Bryllert, Ø. Olsen, **J. Hanning**, and J. Stake, “Monolithic HBV-Based 282-GHz Tripler With 31-mW Output Power,” *IEEE Electron Device Letters*, vol. 33, no. 6, pp. 800–802, June 2012.
- [d] H. Zhao, V. Drakinskiy, P. Sobis, **J. Hanning**, T. Bryllert, A. Y. Tang, and J. Stake, “Development of a 557 GHz GaAs monolithic membrane-diode mixer,” in *Proceedings of IEEE InP Related Materials Conference*, 2012, pp.102–105.
- [e] P. Sobis, V. Drakinskiy, A. Emrich, H. Zhao, T. Bryllert, A. Y. Tang, **J. Hanning**, J. Stake, “300 GHz to 1.2 THz GaAs Schottky membrane TMIC’s for next generation space missions,” presented at *24th International Conference on Space Terahertz Technology*, Groningen, The Netherlands, 2013.

- [f] **J. Hanning**, T. Bryllert, J. Vukusic, A. Ø. Olsen, J. Stake, “HBV MMIC frequency tripler and quintupler for high power THz applications,” in *Millimetre Wave Days Proceedings, The 6th ESA Workshop on Millimetre-Wave Technology and Applications AND The 4th Global Symposium on Millimeter Waves GSMM2011*, Espoo, Finland, May 2011.
- [g] **J. Liljedahl\***, T. Bryllert, J. Vukusic, J. Stake, “Development of a HBV tripler for 0.6 THz,” in *21st International Conference on Space Terahertz Technology*, Oxford, UK, 2010.

\*The author’s name was Liljedahl prior to June 2010.



# Notations and abbreviations

## Notations

$\alpha$	Propagation attenuation constant
$a$	Complex incident traveling wave
$\beta$	Propagation phase constant
$b$	Complex reflected traveling wave
$\gamma$	Propagation constant
$c$	Speed of light
$\eta$	Wave impedance
$E$	Error term
$\mathbf{E}$	Electric field
$\mathbf{E}_t$	Transverse electric field
$f$	Frequency
$f_c$	Cutoff frequency
$\mathbf{H}$	Magnetic field
$\mathbf{H}_t$	Transverse magnetic field
$I$	Current
$k$	Wavenumber
$k_c$	Wavenumber at cutoff frequency
$\lambda$	Wavelength
$\lambda_0$	Wavelength in free-space
$\lambda_g$	Wavelength inside waveguide
$\omega$	Angular frequency
$P$	Power

$S$	Scattering parameter
$V$	Voltage
$\phi$	Phase
$Z$	Impedance
$Z_c$	Characteristic impedance
$Z_{\text{ref}}$	Reference impedance

## Abbreviations

CPW	Coplanar waveguide
DUT	Device under test
ESA	European Space Agency
HEMT	High electron mobility transistor
IL	Insertion loss
InP	Indium phosphide
JUICE	Jupiter Icy Moon Explorer
LO	Local oscillator
LRL	Line-reflect-line
PECVD	Plasma enhanced chemical vapour deposition
RL	Return loss
SOLT	Short-open-load-through
SNA	Scalar network analyzer
TE	Transverse electric fields
TEM	Transverse electro-magnetic fields
THz	Terahertz
THz-TDS	Terahertz time-domain spectroscopy
TM	Transverse magnetic fields
TMIC	Terahertz integrated membrane circuit
TRL	Thru-reflect-line
TSM	Thru-short-match
TS(RO)	Thru-short-radiating-open
VNA	Vector network analyzer
VSWR	Voltage standing wave ratio
WR-1.5	Rectangular waveguide covering 500–750 GHz
WR-03	Rectangular waveguide covering 220–325 GHz



# Contents

Abstract	i
List of publications	ii
Notations and abbreviations	vi
<b>1 Introduction</b>	<b>1</b>
<b>2 THz circuit characterisation</b>	<b>5</b>
2.1 Terahertz integrated membrane circuit technology	5
2.1.1 Waveguide fields and impedance . . . . .	7
2.1.2 Impedance in waveguide circuit theory . . .	8
2.1.3 S-parameters . . . . .	10
2.2 Impedance measurements . . . . .	11
2.2.1 Network analysers . . . . .	12
2.2.2 THz-TDS . . . . .	12
2.3 Parameter extraction and de-embedding . . . . .	12
<b>3 THz S-parameter measurements</b>	<b>15</b>
3.1 THz VNA . . . . .	15
3.2 Measurements . . . . .	17
3.2.1 On-wafer probing . . . . .	17
3.2.2 Waveguide integrated measurements . . . .	18
3.3 VNA error models . . . . .	19

3.4	VNA calibration . . . . .	20
3.4.1	Calibration algorithms . . . . .	21
3.4.2	TRL . . . . .	22
3.5	VNA uncertainty model . . . . .	22
3.6	Sources of measurement uncertainty . . . . .	24
3.6.1	Access waveguide width error . . . . .	25
3.6.2	Flanges . . . . .	27
3.6.3	Mounting related errors . . . . .	28
3.6.4	Test port cable flex . . . . .	28
<b>4</b>	<b>New TRL-kit design and realisation</b>	<b>29</b>
4.1	Design . . . . .	31
4.1.1	Line length . . . . .	31
4.1.2	Access waveguide design . . . . .	33
4.1.3	Residual error simulation . . . . .	36
4.1.4	Block design . . . . .	36
4.2	Terahertz integrated membrane circuit processing .	38
4.3	Circuit measurement results . . . . .	40
<b>5</b>	<b>Conclusion and future outlook</b>	<b>43</b>
<b>6</b>	<b>Summary of appended papers</b>	<b>47</b>
	<b>Acknowledgements</b>	<b>49</b>
	<b>References</b>	<b>51</b>
	<b>Appended papers</b>	<b>59</b>

# Chapter 1

## Introduction

This thesis treats the characterisation of waveguide integrated devices operating in the terahertz (THz) region of the electromagnetic spectrum, and the development of a novel setup for improved measurement uncertainty when characterising integrated membrane circuits.

Terahertz radiation has lower frequency than visible light, but higher frequency than signals commonly used for radar and wireless communication, e.g. mobile phones and Wi-Fi. The term terahertz waves or terahertz radiation often refers to frequencies within 0.1 THz to 10 THz, corresponding to wavelengths of 0.03 mm to 3 mm, including the sub-mm wave region at 0.1 mm to 1 mm.

The possibility to determine the existence of gas molecules, by probing for electro-magnetic radiation in the THz frequency range in various regions of outer space, has made astronomy, planetary and Earth science the driving forces behind THz technology for decades [1,2]. Terahertz wavelengths correspond to rotational and vibrational energy levels in simple molecules, such as water ( $\text{H}_2\text{O}$ ), providing each molecule a unique signature in the THz region of

the electromagnetic spectrum. First observations of pure rotation spectra was in 1925, using THz detection [3]. The ESA space observatory Herschel is one of the latest instruments covering the far infrared to sub-mm spectrum, with which astronomers were able to observe star birth within a massive early Universe galaxy cluster for the first time last year [4]. Moreover future space missions carrying THz instrumentation are planned, such as JUICE – ESA’s mission to Jupiter’s icy moons. JUICE will carry a heterodyne spectrometer (SWI) operating at 0.53 THz to 0.6 THz and 1.08 THz to 1.275 THz, to investigate the composition of the moons’ atmospheres [5].

Recently other advantages of terahertz radiation have been highlighted, such as it’s ability to penetrate materials such as plastic, paper, and fabric, providing descent resolution for imaging while not being ionising like X-rays. This opens up for new applications, such as medical imaging or non-invasive product inspection.

However, while new areas of applications are emerging, terahertz device technology is still under development. Fundamental limitations, such as carrier velocity, limits availability of semiconductor components in the THz range, and existing sources provide low power levels [6]. High frequencies also mean that the effect of parasitic circuit elements (capacitances and inductances) increases, making it more difficult for the circuit designer to match the device. Thus there is a need to measure and verify circuit and device models in the THz regime.

Furthermore, THz device development has been hampered by the lack of measurement technologies operating at these frequencies, which makes device characterisation and modelling difficult. By measuring the phase and amplitude response of a device at its operating frequency, models can be improved for design purposes.

Historically THz measurement techniques were usually broad-

band power measurements using direct detectors. These types of detectors needed to be calibrated with well known sources [7]. A typical broad band sensor used for far infrared (FIR) and terahertz detection in early research was the thermopile, which took a great amount of work and time to get thermally stable before measurements could proceed [3, 8]. These detectors were used in the grating spectroscopy instruments used in the 1920's. After World War II the more sensitive and faster pneumatic detector, the Gollay cell, was invented, advancing the field [3, 8, 9]. For the broader research community, the advent of the Erickson power meter in 2002 was the major breakthrough [10]. Although the power meter is not frequency selective, it provided improved accuracy and measurement results that could be repeated at different institutions.

While power measurements have been available, the lack of necessary sources in the THz region, has made vector measurements, i.e. measurement of magnitude and phase, at THz frequencies challenging. Up to the mid-1980's mostly magnetrons, klystrons and gas lasers are mentioned for millimetre waves, but only gas lasers operate at THz frequencies [3]. The terahertz field was then driven by the photonic research community, and the development of the femtosecond laser made phase and amplitude measurements possible through THz time-domain spectroscopy (THz-TDS) [11]. The first vector network analyser (VNA) working up to 1 THz was presented as late as in 1989, by Philippe Goy [12, 13]. However, Goy's was the only system until the recent development of VNA frequency extenders up to 1.1 THz [14]. Access to VNA frequency extenders means evaluation of parasitic circuit elements, that has only been simulated before, may be performed [15], and new frequency dependent effects predicted in simulation may be verified and modeled [16].

Accurate characterisation at operating frequency is important

for both active and passive THz circuit components. Still, manufacturing tolerances and high uncertainties in calibration provide a challenge for accurate S-parameter characterisation. This thesis started from the need to measure and characterise waveguide integrated devices, such as devices based on terahertz integrated membrane circuit technology, see [17]. In this work, a calibration and measurement setup that reduces measurement uncertainty due to manufacturing tolerances of the access waveguides, has been developed. The setup is used for S-parameter characterisation of waveguide integrated membrane circuits, using a VNA with extenders operating in the WR-03 (220-325 GHz) frequency band. Calibration is done with a specially developed waveguide integrated membrane TRL-kit (thru-reflect-line). The setup improved measurement uncertainty of two different measured passive waveguide devices, with an order of magnitude.

This thesis begins with a brief theoretical background of THz circuit characterisation in chapter 2. In Chapter 3 the THz VNA S-parameter measurement method is described, together with calibration algorithms and the uncertainty model. Finally in chapter 5, the novel TRL-kit is described more in detail.

## Chapter 2

# THz circuit characterisation

In this chapter the THz membrane technology, and the modelling theory related to it described, as well as how THz membrane circuits can be characterised, by measurement and deembedding.

### 2.1 Terahertz integrated membrane circuit technology

Due to the limited available power at terahertz frequencies, waveguides providing low loss, such as hollow rectangular waveguides, see Figure 2.2a, are often preferred over transmission lines to connect THz devices. Planar THz devices such as Schottky diodes are however implemented in transmission line technology, which is then integrated in the hollow waveguide [17]. Figure 2.1 shows for example a Schottky diode membrane THz mixer [18].

Membrane circuits in stripline, or co-planar waveguide (CPW) mode, see Figure 2.2d and Figure 2.2c, provide several advantages

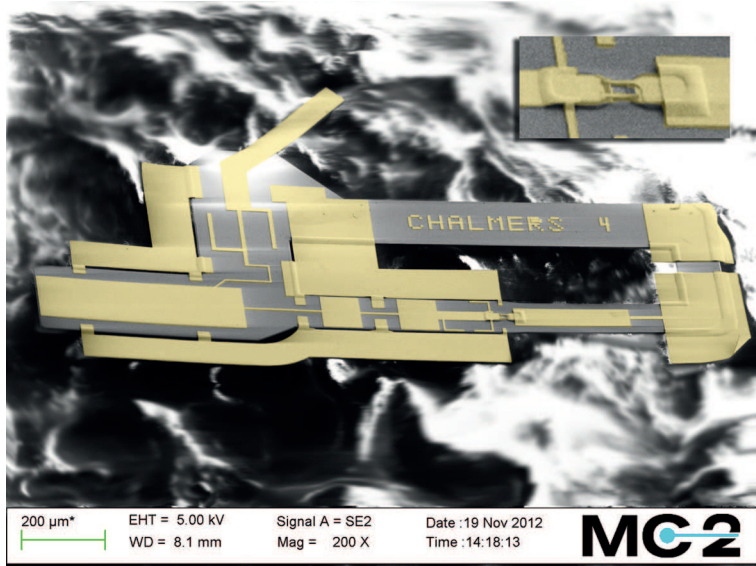


**Figure 2.1:** SEM image of a Schottky diode mixer circuit on membrane technology [18]. The membrane is  $3\ \mu\text{m}$  thick GaAs, and will be mounted inside a waveguide block.

over for example microstrip, see Figure 2.2b, in the waveguide integrated environment. The thin membrane facilitates lower loss compared to thicker substrates, and the manufacturing process of membranes provides a better controlled thickness. But more importantly, membranes reduce the risk of signal leakage via substrate waveguide modes, that may otherwise pass through high permittivity substrates [19]. In addition, shrinking of enclosing waveguide dimensions is often necessary to cut off waveguide modes.

For membrane CPW or stripline mode transmission lines, the result is often that the field couples not only to the conductor and ground planes, but also to the waveguide walls, see Figure 2.2c and Figure 2.2d. Therefore, the enclosing waveguide is an integral part of the device, that also needs to be included in device

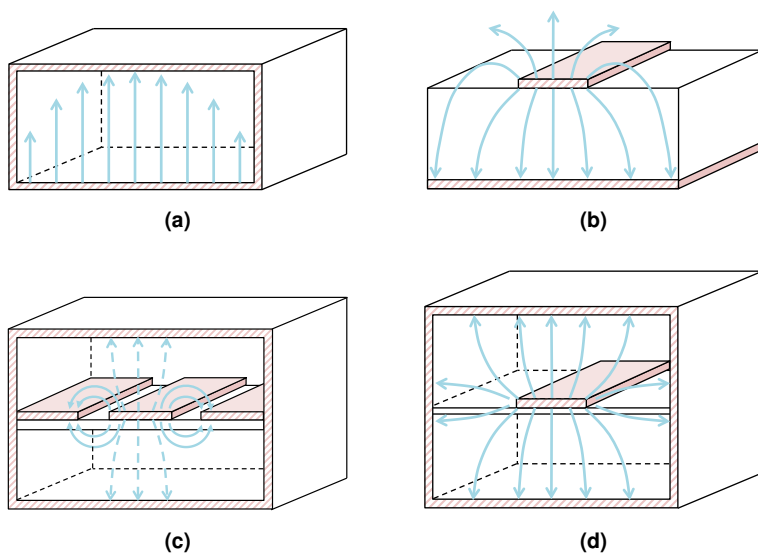


**Figure 2.2:** Image of the E-fields in the first order modes for different type of waveguides: (a) Rectangular waveguide, (b) microstrip, (c) waveguide integrated membrane CPW, and (d) waveguide integrated membrane suspended strip line.

characterisation. Thus making it unsuitable to measure devices with on-wafer probing.

### 2.1.1 Waveguide fields and impedance

At high frequencies, where the size of waveguides and circuit components are in the same order as the wavelength, the traveling wave may be described by the propagating electromagnetic fields. This is advantageous since current and voltages are not easily measured, and may not even be uniquely defined in the waveguide. Due to the complexity of the waveguide integrated membrane circuit, this is often the preferred method of modelling.

The solutions to the boundary value problem of Maxwell's equations for a traveling wave is either transverse electromagnetic

(TEM), transverse electric (TE), or transverse magnetic (TM) mode. TEM modes propagate on a transmission line, where there are at least two conductors, and there is no field component parallel to the propagation axis of the waveguide. TE and TM modes are split up in several eigenvalue solutions to the boundary value problem. For TE there is a magnetic field component in the direction of propagation, moving the wave forward, and vice versa for TM waves. With the  $z$ -axis in the direction of propagation of the waveguide the propagating electric and magnetic field waves are

$$\mathbf{E}(x, y, z) = \mathbf{E}_t(x, y)e^{-\gamma z} + \mathbf{E}_t(x, y)e^{\gamma z} \quad (2.1)$$

and

$$\mathbf{H}(x, y, z) = \mathbf{H}_t(x, y)e^{-\gamma z} - \mathbf{H}_t(x, y)e^{\gamma z} \quad (2.2)$$

where  $\gamma = \alpha + j\beta$  is the propagation constant. As can be seen in Figure 2.2d the electric field of the first order mode of a suspended stripline on membrane is almost a coaxial mode. If the enclosing waveguide is narrow, it is the same for the waveguide integrated CPW on membrane, see Figure 2.2c.

The traveling wave can be described by the wave impedance. This impedance is mode specific, and defined by the ratio of the transverse electric  $\mathbf{E}_t$  and magnetic field  $\mathbf{H}_t$  of this mode. The wave impedance for mode  $n$  then becomes

$$\eta_n = \frac{\mathbf{E}_{t,n}}{\mathbf{H}_{t,n}}. \quad (2.3)$$

For a plane wave in free space  $\eta_0 = \sqrt{\mu_0/\epsilon_0} \approx 377 \Omega$ .

## 2.1.2 Impedance in waveguide circuit theory

Although the electromagnetic field solutions are a more accurate model of the waveguide, there are many similarities between wave-

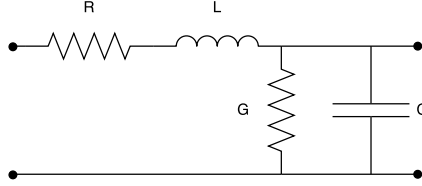


**Figure 2.3:** Waveguide lumped element equivalent circuit.

guide circuits and the electrical circuits that obey Kirchhoff's laws, why it is also practical to describe the device in terms of equivalent circuits and impedance [20]. A section of a waveguide may be modeled as an equivalent circuit of lumped elements, i.e. elements that are much smaller than the wavelength in size, such that the voltage and current over the device is constant, see Figure 2.3.

The current and voltages of traveling waves depend on their definition and normalisation, and are related to the intensities of the electric and magnetic fields via the characteristic impedance of the propagating mode [21]. This means that the characteristic impedance also is determined by how it is defined. Three commonly used definitions are these, introduced by Schelkunoff

$$Z_{c,VI} = \frac{V}{I}, \quad Z_{c,PI} = \frac{2P}{|I|^2}, \quad \text{or} \quad Z_{c,PV} = \frac{|V|^2}{2P^*}, \quad (2.4)$$

where the asterisk denotes complex conjugate,  $V$  and  $I$  voltage and current respectively, and  $P$  the power [20]. The different impedances are related as

$$Z_{c,PI} Z_{c,PV}^* = |Z_{c,VI}|^2, \quad (2.5)$$

but for TEM waves

$$Z_{c,PI} = Z_{c,PV} = Z_{c,VI}. \quad (2.6)$$



**Figure 2.4:** 2-port scattering matrix

By introducing the concept of impedance in both electromagnetic field and waveguide circuit theory, the two theories can be joined.

### 2.1.3 S-parameters

In practice neither the fields nor the impedance, voltage or currents in a wave guiding system are measurable at high frequencies. Instead if we want to characterise a device in a wave guiding system, we are left with measurements of the magnitude and phase of the transmitted and reflected waves. The transmitted and reflected power of a device is most often described by the device scattering parameters (S-parameters).

Since the currents, voltages and electromagnetic fields are inaccessible experimentally, the scattering matrix is a very useful tool when determining the impedance. Pseudo waves at port  $n$  can be defined as [21]

$$a_n(Z_{\text{ref}}^n) = \left[ \frac{|v_0| \sqrt{\text{Re}(Z_{\text{ref}}^n)}}{v_0 2|Z_{\text{ref}}^n|} \right] (v + iZ_{\text{ref}}^n) \quad (2.7)$$

and

$$b_n(Z_{\text{ref}}^n) = \left[ \frac{|v_0| \sqrt{\text{Re}(Z_{\text{ref}}^n)}}{v_0 2|Z_{\text{ref}}^n|} \right] (v - iZ_{\text{ref}}^n), \quad (2.8)$$

where  $Z_{\text{ref}}^n$  is the reference impedance at each port, and  $v$  and  $i$  the corresponding voltage and current. If  $Z_{\text{ref}}^n = Z_c^n$ , the pseudo waves become the traveling waves. There are other definitions of

the same quantities, often also called power waves [22, 23]. Then, with the incident and reflected waves as in (2.7) and (2.8), the scattering matrix of a 2-port is

$$\begin{bmatrix} b_1 \\ b_2 \end{bmatrix} = \begin{bmatrix} S_{11} & S_{12} \\ S_{21} & S_{22} \end{bmatrix} \begin{bmatrix} a_1 \\ a_2 \end{bmatrix}. \quad (2.9)$$

And if the reference impedance is equal to the characteristic impedance for each port, the pseudo matrix becomes the regular scattering matrix.

In addition to determining the impedance, the S-parameters determine other useful parameters of waveguide components. For a 2-port we have:

Insertion loss at port 1

$$IL = -20 \log_{10} |S_{21}| \quad (2.10)$$

and return loss at the same port

$$RL = -20 \log_{10} |S_{11}|. \quad (2.11)$$

## 2.2 Impedance measurements

Traditional impedance measurement technologies, where either the current-voltage relationship over a device is measured, or the impedance by tuning out an AC signal with variable known impedances, commonly known as LCR-meters, are only available up to about 3 GHz. Above 3 GHz the network analysis method is used, where instead the incident and reflected waves on the DUT are measured, with corresponding S-parameters.

In general, one may say that the LCR-meters are available at frequencies where the devices are considered lumped elements, while network analysers are used where the waveguide circuit the-

ory applies. Another method to determine the impedance by measuring the incident and reflected waves at THz frequencies is terahertz time-domain spectroscopy (THz-TDS).

### 2.2.1 Network analysers

Network analysers are divided into two different categories, scalar network analysers (SNA) and vector network analysers (VNA). SNA only measure the amplitude ratio of the incident and reflected or transmitted waves. For phase information, one can use a 6-port reflectometer [24] or a VNA.

Most VNAs for two port measurements have four receivers, that measure the magnitude and phase of the incident and reflected signal at each port. They rely on the availability of mixers or samplers, and LO-sources operating at THz frequencies. There are also VNA based on the 6-port reflectometer. The 6-port reflectometer in itself uses four direct power detectors to sample the standing wave, and determine both amplitude and phase of the ratio of the incoming and reflected waves [25].

### 2.2.2 THz-TDS

Both amplitude and phase information of the incident and reflected wave can also be measured in a THz-TDS system [11, 26]. THz-TDS is a photonics technology, based on the femto-second laser.

## 2.3 Parameter extraction and de-embedding

When performing measurements to determine the impedance of a device, the measurement location is normally separated from the

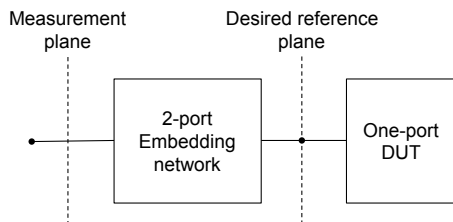


**Figure 2.5:** One port measurement situation, where the actual measurement plane is separated from the desired [27].

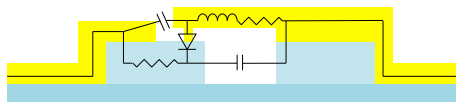


**Figure 2.6:** Planar Schottky diode with equivalent circuit of parasitic elements. Yellow = gold conductor, blue = semiconductor.

device by some intervening structure, also known as an embedding structure [27], see Figure 2.5. Often the impedance of the embedding structure needs to be characterised, in order to remove it from measurements, i.e. de-embedding to the DUT. The embedding structure may also be an integral part of the device, that its properties need to be known for performance purposes. For example for a planar Schottky diode, a change in the size of the anode, which affects the intrinsic device properties, results in a change of the contact width, resulting in a higher stray capacitance in the embedding circuit [28], see Figure 2.6.

Models of active semiconductor devices are based on measurements of these devices under controlled conditions. To obtain the most accurate model, the devices need to be measured at the operating frequency. Figure 2.5.



## Chapter 3

# THz S-parameter measurements

In this chapter THz S-parameter measurement technology using a vector network analyser is described. A brief description of the VNA itself is followed by a description of on-wafer and waveguide integrated measurement setups. The VNA error models and different calibration techniques are also described, with focus on the TRL algorithm, as well as a description of a method for analysing measurement uncertainty, and examples of what the major sources of uncertainty are at THz frequencies.

### 3.1 THz VNA

As mentioned in chapter 2, the VNA measures both amplitude and phase of the incident, transmitted and reflected waves.

Figure 3.1 shows a simplified block diagram of a 4-sampler VNA. Directional couplers couple a fraction of the incident signal to the receiver  $m_1$  as a signal reference. The reflected signal from the DUT,  $b_1$  is coupled to and measured at the receiver  $m_2$ . The

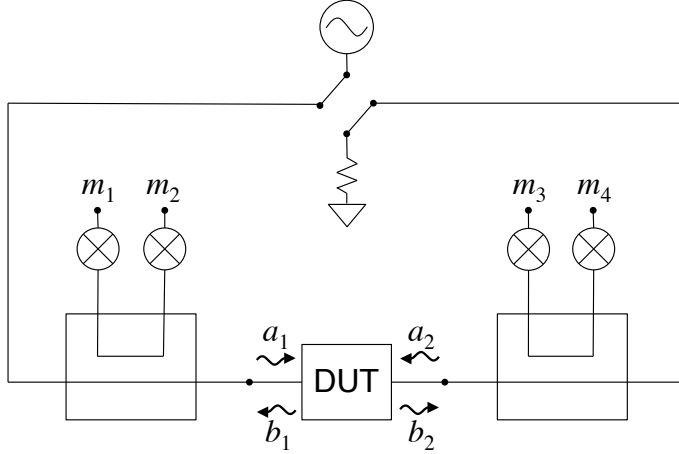


**Figure 3.1:** Simplified VNA block diagram.

same way, the transmitted signal  $b_2$  is coupled to and measured at receiver  $m_3$ .

If the incident signal at port 2 is  $a_2 = 0$ , ideally, the measured signal ratios would correspond to the incident, reflected and transmitted signal ratios

$$\frac{m_2}{m_1} = \frac{b_1}{a_1} \Big|_{a_2=0} = S_{11} \quad (3.1)$$

$$\frac{m_3}{m_1} = \frac{b_2}{a_1} \Big|_{a_2=0} = S_{21}. \quad (3.2)$$

However, in reality this is never the case. The directional couplers are not ideal, and cross coupling of the signal between the ports will occur. Additionally, connectors, cables and other components are not ideal, and will cause reflections, attenuation and phase distortion. In order to measure our device, we need to characterise the entire system and correct for these effects from the measurement.

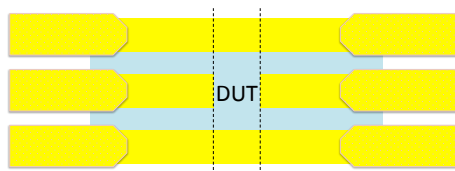


**Figure 3.2:** Illustration of co-planar on-wafer probes.

The purpose of calibration is to characterise the systematic errors, from the VNA itself or components such as cables, connectors, etc. Calibration will not take care of random errors, errors that are time dependent, such as noise, thermal variations, and connection repeatability.

## 3.2 Measurements

At THz frequencies there are a few ways to connect the device under test (DUT), for example on-wafer probing or on waveguide integrated membrane.

### 3.2.1 On-wafer probing

On-wafer probed measurements, see Figure 3.2, is the most common technique at frequencies up to about 110 GHz [29]. A big advantage is that single components can be characterised without dicing and mounting, allowing for industrial process testing. By calibration, the measurement reference plane can be put at the probe tips or on the transmission line, closer to the DUT.

In spite of the many advantages of on-wafer probing, it is only recently that probes working at THz frequencies have been developed [30,31]. Moreover, recently published THz on-wafer measurement results (at 325 GHz to 508 GHz and 325 GHz to 750 GHz) shows ripples in the measurement results due to unintentional

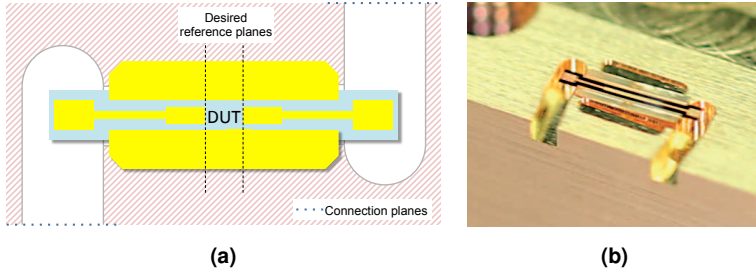


**Figure 3.3:** (a) WR-03 Waveguide integrated membrane, regular block [33]. (b) Waveguide integrated membrane with access waveguides in one flange [Paper A].

propagating substrate modes [31], and phase uncertainty due to probe misalignment [32].

Both problems arise from the short wavelength of the THz waves. Substrates need to be thinner in order to avoid substrate waveguide modes for higher frequencies, and at THz frequencies the probe misalignment ( $\Delta z \approx 5 \mu\text{m}$  [32]) and wavelengths become comparable in size. Thus causing a noticeable phase error.

### 3.2.2 Waveguide integrated measurements

For suspended stripline technology, or membrane circuit technology, waveguide integrated measurements are necessary, since the waveguide itself is part of the device. A setup for using TRL calibration on membrane circuits was proposed in [33, 34], see Figure 3.3a. And an alteration of this setup was proposed in [Paper A, Paper B], see Figure 3.3b.

For characterisation of waveguide integrated components the calibration reference plane and the connection plane to the measurement device for the device under test (DUT) are separate [33], see Figure 3.4. In this case an embedding structure is included in both the DUT and the calibration standards. Here, the circuitry between one reference plane and the corresponding connection

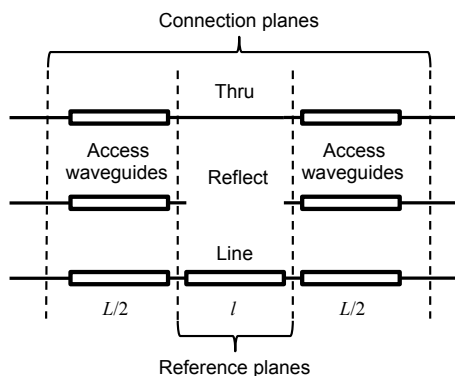


**Figure 3.4:** Thru, Reflect and Line standards where the calibrated reference planes and connection planes are separated by access waveguides on each side [Paper A].

plane is called access waveguide. Although the access waveguides are, in theory, eliminated by the calibration, differences between the access waveguides in the different calibration standards and the DUT give rise to calibration uncertainty, [35, 36].

It is also possible to calibrate the measurement at the waveguide interface. But, the measured result may be much less accurate, since the access waveguides will be included in the measurement.

### 3.3 VNA error models

Error models are used to describe the systematic errors introduced by the VNA. By determining the terms of the error models through measurement of known devices, the errors resulting from the VNA and connecting waveguides, can be removed from the DUT measurements. There are 8, 12 and 16 term error models for 2-port measurements.

The 8 term error model is the most basic go the Three models,

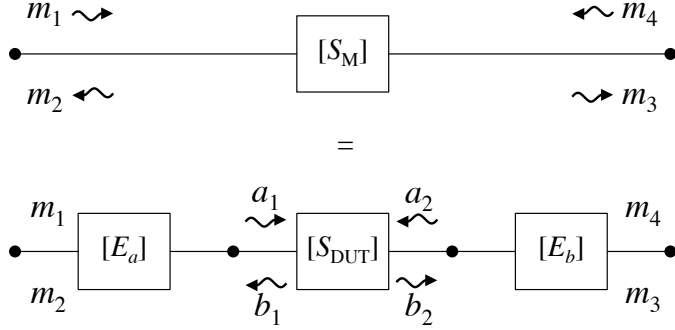


**Figure 3.5:** Deembedding, 8 error term model

where zero leakage between the measurement ports is assumed, see Figure 3.5. This is usually enough for the waveguide integrated circuits, where the waveguide cuts of most stray fields coupling the measurement ports. The S-parameter error boxes are

$$\mathbf{E}_a = \begin{bmatrix} E_{00} & E_{01} \\ E_{10} & E_{11} \end{bmatrix} \quad \text{and} \quad \mathbf{E}_b = \begin{bmatrix} E_{22} & E_{23} \\ E_{32} & E_{33} \end{bmatrix} \quad (3.3)$$

In 12-term and 16-term error models, leakage paths are considered. In the 12 term error model the forward and reverse measurements are modelled separately. The 16-term error model is an expansion of the 8 error term model, where the error box is one 4-port rather than two 2-port error boxes.

### 3.4 VNA calibration

Calibration consists of measuring on a set of known standards in order to determine the terms in the error models, and the subsequent removal of the error terms from the VNA measurements. There are several calibration algorithms, and they are named after the standards, that are used in order to determine the error terms.

The standards are more or less well known devices, for example a through (T or thru) connection, a delay line (L or line), or a reflect standard (R) realised by an open or short circuit. There are also radiating open (RO) and match (M) standards that provide a match to the circuit. The algorithm used, determines by which level the standards need to be known.

### 3.4.1 Calibration algorithms

A very common calibration algorithm is the thru-reflect-line (TRL) calibration, first suggested by Engen and Hoer [37]. A big advantage is that the standards behaviour need only to be partly known. There exist variations of the TRL algorithm, for example LRL and LRM, where a second delay line or a match standard is used instead of the thru connection. They determine the 7 independently known parameters that must be measured in the 8 error term model.

At high frequencies waveguide calibration becomes sensitive to fabrication and alignment tolerances. In [38] WR-1.5 rectangular waveguide thru-reflect-line (TRL) calibrations at 500–750 GHz are compared with thru-short-match (TSM) and thru-short-radiating-open (TS(RO)) calibrations. The latter two were shown to be less sensitive to systematic bias errors that cannot be eliminated by averaging, than the TRL algorithm.

There also exist calibration algorithms that may be more common at lower frequencies or when using higher order term error models, such as SOLT, i.e. short-open-load-thru, presented in [39]. The SOLT standards need to be well known, i.e. each standard's behaviour is known through data or models, and are usually realised in coaxial transmission line.

### 3.4.2 TRL

As mentioned above, the advantage of the TRL algorithm is that the standards behaviour need not be fully known. This means that they are easier to realise. The requirement is that there is no reflection for the thru and line, i.e.  $S_{11} = S_{22} = 0$  for both standards, and that the reflect standard is equal at both ports. A consequence of the former requirement is that the TRL calibration automatically sets the system reference impedance to the characteristic impedance of the line. In addition, it is necessary to know if the phase delay provided by the line standard is in the upper or lower half plane on the unit circle, but it must not be  $\phi = \gamma l = n\pi, \forall n \in \{0, 1, 2, \dots\}$ .

The S-matrix of the calibration standards thru  $\mathbf{S}_T$ , reflect  $\mathbf{S}_R$ , and line  $\mathbf{S}_L$  are [40]

$$\mathbf{S}_T = \begin{bmatrix} 0 & 1 \\ 1 & 0 \end{bmatrix} \quad (3.4)$$

$$\mathbf{S}_R = \begin{bmatrix} \Gamma_R & 0 \\ 0 & \Gamma_R \end{bmatrix} \quad (3.5)$$

$$\mathbf{S}_L = \begin{bmatrix} 0 & e^{-\gamma l} \\ e^{-\gamma l} & 0 \end{bmatrix} \quad (3.6)$$

The TRL algorithm may be further improved by the use of multiple line lengths, which results in a more wide band calibration and less measurement uncertainty [41, 42].

## 3.5 VNA uncertainty model

The error boxes determined through calibration, can only be estimated with a certain amount of uncertainty. A way to account for uncertainties in the error model is by introducing residual errors [43]. Instead of the ideal error S-parameter matrix in Figure

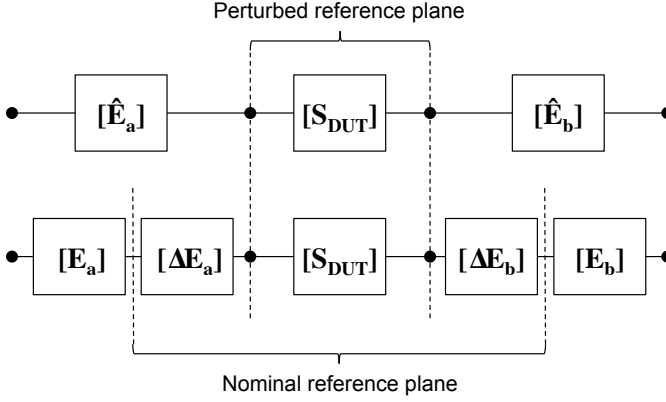


**Figure 3.6:** Uncertainty model of VNA, 8 term error model with residual errors [36].

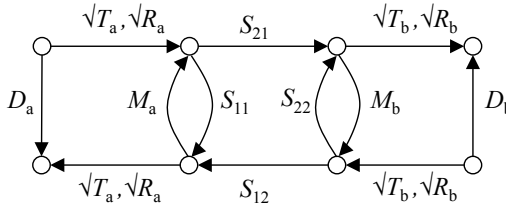


**Figure 3.7:** Residual error model for S-parameter measurements [44].

3.5, we have an estimated error matrix  $\hat{\mathbf{E}}_{\mathbf{a},\mathbf{b}}$  that can be treated as a residual error matrix  $\Delta \mathbf{E}_{\mathbf{a}}$  in cascade with the true error matrix  $\mathbf{E}_{\mathbf{a}}$ ,

$$\hat{\mathbf{E}}_{\mathbf{a}} = \mathbf{E}_{\mathbf{a}} \otimes \Delta \mathbf{E}_{\mathbf{a}} \quad (3.7)$$

where  $\otimes$  denotes a cascade connection, see Figure 3.6. As long as we don't know the true error terms, the residual errors can only be an estimate. However, it is a useful concept in simulations and analysis of uncertainties caused by known perturbations.

The residual errors are evaluated in terms of residual directivity,  $D$ , match,  $M$ , and reflection and transmission tracking,  $R$  and

$T$ , see Figure 3.7. The residual directivity is given by

$$D_a = \Delta E_{a,11} \quad \text{and} \quad D_b = \Delta E_{b,22}, \quad (3.8)$$

and residual match

$$M_a = \Delta E_{a,22} \quad \text{and} \quad M_b = \Delta E_{b,11}. \quad (3.9)$$

Reflection tracking

$$R_a = \Delta E_{a,12} \Delta E_{a,21} \quad \text{and} \quad R_b = \Delta E_{b,12} \Delta E_{b,21}, \quad (3.10)$$

and transmission tracking

$$T_a = \Delta E_{a,21} \Delta E_{b,21} \quad \text{and} \quad T_b = \Delta E_{a,12} \Delta E_{b,12}, \quad (3.11)$$

where  $T = T_a = T_b$  [36].

There also exists other models for the uncertainty [45].

## 3.6 Sources of measurement uncertainty

In waveguide integrated technology there are many sources of measurement uncertainty related to mounting, connection repeatability and manufacturing tolerances. These become more evident at frequencies approaching THz, as the tolerances become comparable to the wavelength in size.

The waveguide width error has been shown to produce a large uncertainty in the measured phase [35, 36]. And for this reason, a new measurement setup for characterising waveguide integrated membrane circuits has been presented in [Paper A, Paper B]. Other examples of dimensional errors causing measurement uncertainties in waveguide integrated measurements are mounting

misalignment of the membrane circuit or the waveguide block halves, connecting flange misalignment, membrane and waveguide manufacturing tolerances.

There are also random sources of measurement uncertainty, that become particularly important at terahertz, such as phase errors due to cable flexing of the frequency extender cables to the VNA [38]. These type of errors can not be corrected for with calibration, but must be considered in a measurement setup.

### 3.6.1 Access waveguide width error

In [35] it was shown that the product of the width tolerance and the length of the access waveguide impacts the phase uncertainty. The most common technique for fabricating waveguides is by milling the waveguide from a brass block split in half. The split is along the E-plane in the centre of the rectangular waveguide long edge. This means that the manufacturing width tolerance is set by how well the depth of the milling can be defined, and the depth is often difficult to control and measure.

For rectangular waveguide in TE<sub>01</sub> mode the propagation phase constant is

$$\beta = \sqrt{\left(\frac{2\pi f}{c_0}\right)^2 - \left(\frac{\pi}{w_x}\right)^2} \quad (3.12)$$

where  $w_x$  is the waveguide width. Thus a change of the waveguide width will cause a change in the electrical length of the waveguide. The phase delay of the TRL line standard with access waveguides is

$$\phi = \beta_{\text{Line}}(L + l) - \beta_{\text{Thru}}L, \quad (3.13)$$

where  $L$  is the total access waveguide length, and  $l$  is the length of the line standard [35].

And if there is a width difference  $\pm\delta w_x$  between the access

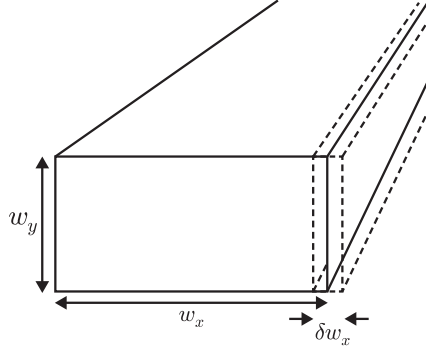


**Figure 3.8:** Waveguide width error.

waveguides for the line and thru standard, a worst case phase error estimation can be obtained by

$$\phi \pm \delta\phi = (L + l) \sqrt{\left(\frac{2\pi f}{c_0}\right)^2 - \left(\frac{\pi}{w_x \pm \delta w_x}\right)^2} - L \sqrt{\left(\frac{2\pi f}{c_0}\right)^2 - \left(\frac{\pi}{w_x \mp \delta w_x}\right)^2}. \quad (3.14)$$

And in terms of residual errors, i.e. residual reflection and transmission tracking,  $R$  and  $T$ , the phase error is

$$\angle R_{a,b} \approx -\frac{2\sqrt{2}\pi L}{w_x^2 F} \delta w_x \quad (3.15)$$

and

$$\angle T_{a,b} \approx -\frac{2\sqrt{2}\pi L}{w_x^2 F} \delta w_x \quad (3.16)$$

where  $F = \sqrt{\left(\frac{f}{f_c}\right)^2 - 1}$ , [36]. The error becomes larger closer to the cutoff frequency.

It becomes evident that the access waveguides length needs to be as short as possible, and width tolerances as tight as possible,

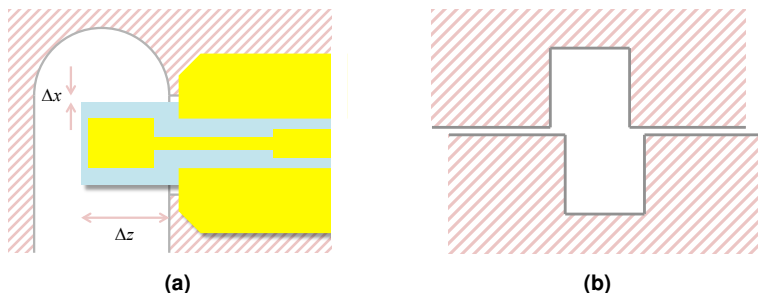


**Figure 3.9:** (a) Membrane circuit alignment in rectangular waveguide. (b) Waveguide block halves misalignment.

to minimise the phase uncertainty. For the setup in [36], with the same width tolerance, the total length of the access waveguides need to be shortened by a factor 6 for the uncertainty contribution to be in the same order as other contributions investigated. That means the total length would have to be reduced from 20 mm to 3 mm in WR-03 waveguides. This was accomplished in [Paper A, Paper B]

### 3.6.2 Flanges

THz waveguide measurements rely on the repeatability of the connection between the different calibration standards and DUT. Much effort is put into investigating the interface and repeatability, for example in [38, 46, 47].

The waveguide displacement at the interface and repeatability has shown that axial displacement cause less error than displacement in x-y [46, 48]. An that the displacement along the waveguide height has the most influence on measurement uncertainty [36, 48]

### 3.6.3 Mounting related errors in waveguide integrated membrane technology

The assembling of membrane circuits in waveguides is subject to mounting tolerances, that affect the calibration and measurement result. The uncertainty, caused by misalignment of the waveguide block halves and membrane probes and circuit, see Figure 3.9, in the calibration standards, propagated through the TRL algorithm, has been investigated by Stenarson et. al. in [36]. In their setup they use E-plane split blocks with E-plane probes as transition between the WR-03 rectangular waveguide and the membrane circuit. The membrane in plane misalignment only gave rise to small changes in the return loss, while block half misalignment perpendicular to the membrane waveguide channel was noticeable [36].

### 3.6.4 Test port cable flex

A known prominent source of measurement uncertainty is flexing of the test port cables connecting the VNA to the DUT or frequency extender [38, 49, 50]. In [38] it was shown that the phase of the signal changed, when the cables connecting the VNA to the frequency extenders were moved, and that the phase error persisted even after repositioning the extenders and cables.

Since the error caused by cable flex is mostly random, rather than systematic, it will not be eliminated by calibration. On the contrary, an error is added with each change of calibration standard.

Various techniques have been suggested to increase repeatability, and thereby the systematic behaviour, by for example limiting cable movement in different directions [38, 49, 50]. However, the best way to limit the measurement errors due to cable flex is by not moving the cables at all, as suggested in [Paper A, Paper B].

## Chapter 4

# New TRL-kit design and realisation

In this work a new TRL-kit and measurement setup was developed, in which the calibration standards and DUT are put in waveguide blocks with both ports in the same flange, i.e. a single flange 2-port, see Figure 4.1 [Paper A, Paper B].

As previously mentioned, the access waveguides need to be shortened to reduce the phase uncertainty caused by manufacturing tolerances. Conventional waveguide blocks, put the inputs in different flanges on opposing sides of the waveguide block. For lower frequencies the waveguides can be made relatively short (a couple of wavelengths) without the block becoming unpractically thin. However for THz frequencies the sizes shrink rapidly, for WR-03 the flange to flange distance would have to be only a couple of millimetres.

A way to circumvent this is by putting the two waveguide ports in the same flange, which allows for short access waveguides without affecting the outer dimensions of the waveguide block. The DUT and standards are connected to the VNA frequency

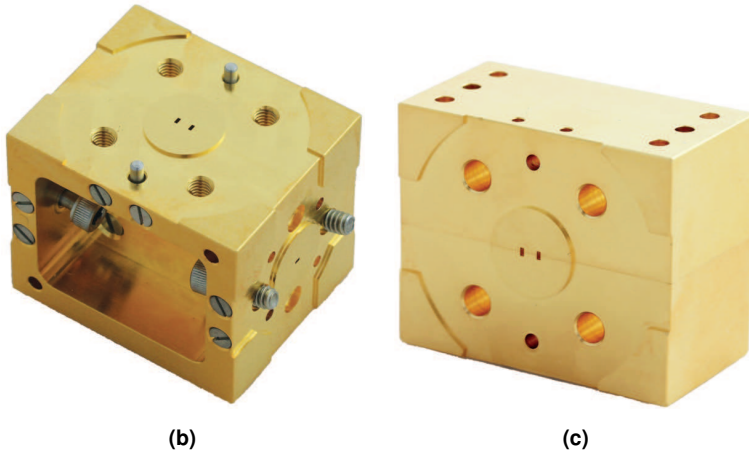
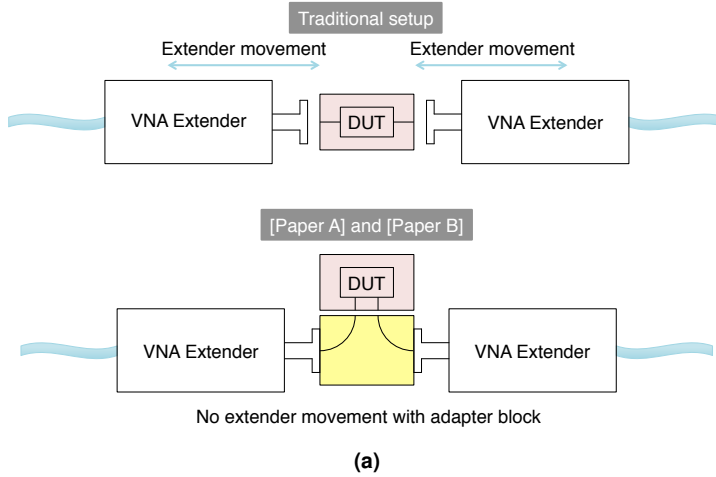


**Figure 4.1:** (a) Traditional vs. new setup. In the traditional setup, VNA extenders were moved when changing the DUT fixture (pink). In the new setup, an adapter block (yellow) connects the extenders to the DUT, and the DUT fixture can thereby be exchanged without any extender movement.

And the new TRL kit, consisting of: (b) Adapter block with a 2-port output in a single flange. (c) Intergangeable 2-port single flange DUT fixture that contains either DUT or the different calibration standards in Figure 4.2.

extenders via an adapter block, which also keeps the extenders locked in position, thereby also eliminating the effects of extender cable flex.

## 4.1 Design

In the new single flange 2-port design, the waveguide inputs at the interface must be at the same distance for all blocks. This forces us to introduce bends in the access waveguides, to accommodate DUTs and TRL standards of different lengths. By a proper choice of line and DUT lengths, we can have the same bends in all standards, only with different orientations, see Figure 4.2. Without this consideration, the access waveguides would have been different between the calibration standards, causing large residual errors.

### 4.1.1 Line length

In the TRL algorithm, the desired phase change that the line standard produces in the transmission coefficient is  $90^\circ$  at the center frequency, relative the thru standard. This corresponds to the line length  $l = \lambda/4$ . However, the algorithm works well with line lengths providing other values of the phase change as long as multiples of  $\lambda/2$ , where the algorithm is ill conditioned, are avoided. A rule of thumb is that the phase change should lie within  $20^\circ$  to  $160^\circ$ , see Figure 4.3. Higher order multiples of  $\lambda/4$  may also be used, so that  $l = (2n + 1)\lambda/4$ . But the longer lines result in a more narrow frequency range to be covered within the allowed phase change [51].

In our TRL-kit design, there are two possible line lengths, depending on if only one or both access waveguide bends are turned outwards, see Figure 4.2. The Line 2 standard will add double the

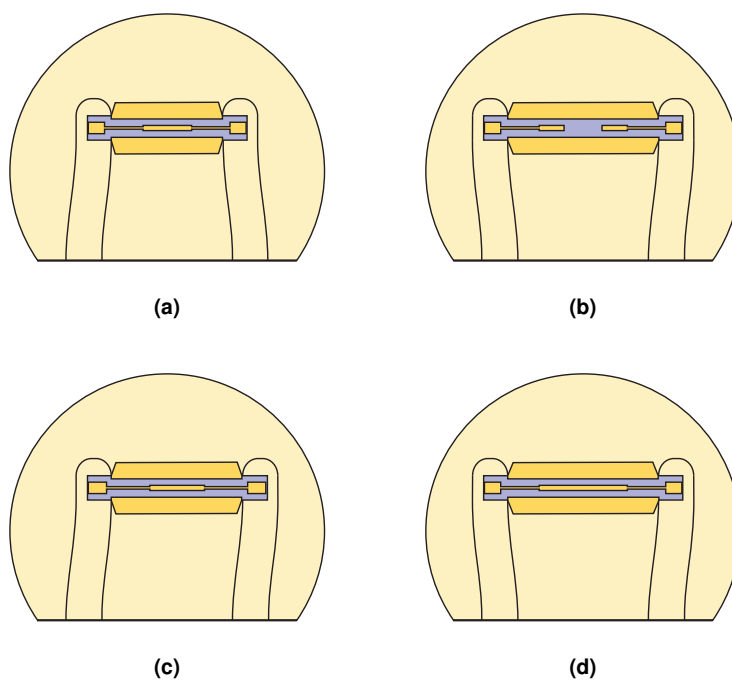


**Figure 4.2:** TRL calibration standards: (a) Thru, (b) Reflect, (c) Line 1, and (d) Line 2.

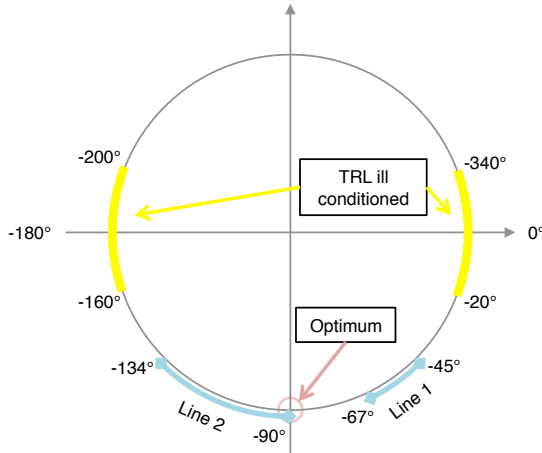


**Figure 4.3:** Phase delay of line standards Line 1 and Line 2 at 220 GHz to 325 GHz in [Paper A] and [Paper B]. Picture also illustrates the “ill conditioned” and optimum points for phase delay of generic TRL line standards.

length of Line 1, compared to the Thru standard. We chose the line lengths so that they both produce a phase change that lies within  $20^\circ$  to  $160^\circ$ , for the entire WR-03 frequency band, and that the average phase shift was  $90^\circ$ . Since the Thru has zero length, the resulting line lengths were  $142\ \mu\text{m}$  and  $284\ \mu\text{m}$ . For Line 1 this corresponds to a phase change within  $45^\circ$  to  $67^\circ$ , and for Line 2  $90^\circ$  to  $134^\circ$ , see Figure 4.3 and [Paper A]. This means that the two bends introduced in the access waveguides, must produce a  $142\ \mu\text{m}$  length difference in the lines.

### 4.1.2 Access waveguide design

According to the previous discussion, the bends need to introduce a line length difference of  $142\ \mu\text{m}$  while keeping the input flange holes distance constant, and the access waveguides as short as possible. The sharper the bends, i.e. the smaller the bend radius,

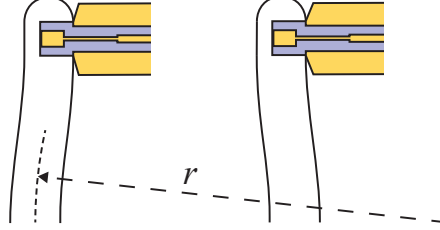


**Figure 4.4:** Bend radius of right and left bent access waveguides.

the shorter the access waveguides will be, see Figure 4.4. But the sharper bends introduce larger reflections and phase difference at the waveguide to membrane transition. These reflections differ slightly depending on the orientation of the bends, thus causing residual errors. A trade-off must be made between waveguide bend radius and phase error due to waveguide width error, which increases for longer access waveguide lengths.

This trade-off was investigated by deembedding the transition parameter  $S_{21}$  of the different access waveguide variations from one another

$$\Delta S_{21} = S_{21,jkl}(X_j, \Delta w_{x,k}, r_l) \cdot S_{21,pqr}^{-1}(X_p, \Delta w_{x,q}, r_r), \quad (4.1)$$

The S-parameters in (4.1) were acquired from 3D FEM high frequency EM simulations, see Figure 4.5, where three different bend radius and width errors, for bends  $X \in \{\text{Left}, \text{Right}\}$ , were introduced:  $\Delta w_x \in \{0 \mu\text{m}, \pm 10 \mu\text{m}\}$ ,  $r \in \{0.6w_y, 6w_y, 10w_y\}$ .  $w_x$  is the waveguide width and  $w_y$  the waveguide height. The signal is coupled from the rectangular waveguide to the membrane circuit via an E-plane probe, at a distance from the waveguide back short where there is a standing wave power maximum. In order to compare the new TRL-kit with the setup in [33,34,36], the waveguide

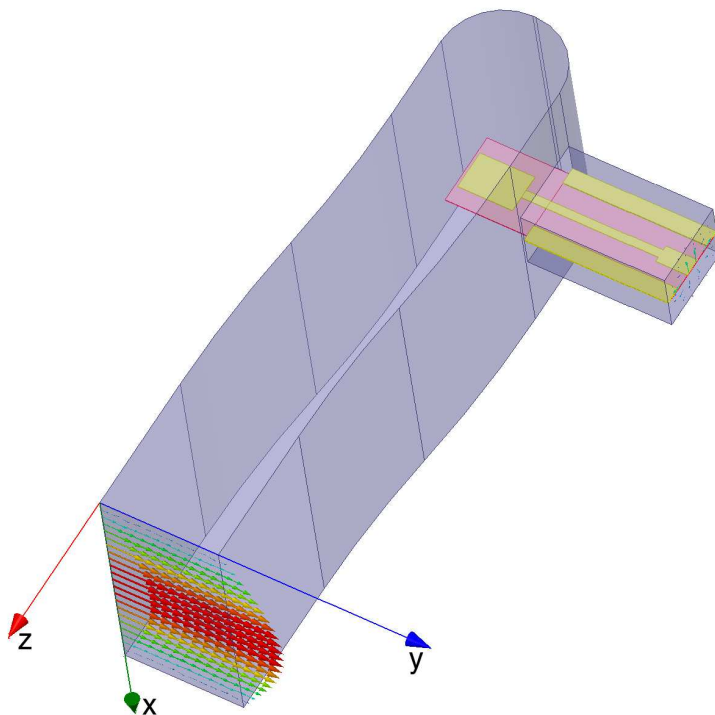


**Figure 4.5:** Access waveguide model 3D setup for full EM simulations in FEM solver, with E-field plotted at the ports.

to membrane transition is exactly the same in both setups. The exported S-parameters were then de-embedded using a Python script.

Of the three different bend radius investigated in [Paper B] it was determined that a waveguide bend radius of  $6w_y$  was optimal. This results in a total access waveguide length of about 2.6 mm, which would have been very difficult to realise in the traditional setup, with access waveguides on opposing sides of the waveguide block.

### 4.1.3 Residual error simulation

The membrane circuit sections containing the thru, reflect, and two lines, were also simulated in the 3D FEM high frequency EM solver, and the exported S-parameters cascaded with the access waveguides to achieve all possible standard variations, see Figure 4.2, for the bend radius of  $6w_y$ . An “ideal” set of standards was also formed, where all have the same access waveguides.

Next, the calibration algorithm was run, using all different standard variations, to determine the calibration error matrixes in (3.3). The residual errors could then be determined through comparison with the error terms of the ideal set, according to (3.7). And residual directivity, match, and reflection and transmission tracking computed with (3.8), (3.9), (3.10) and (3.11).

The phase of the reflection tracking was estimated to lie within  $-8^\circ$  to  $12^\circ$ , see Figure 3 in [Paper B].

### 4.1.4 Block design

The TRL-kit and adapter block was manufactured in brass blocks, using high precision milling, and plated with gold. Detailed drawings of the block are presented in Figure 4.6 and Figure 4.7. The 2-port flange design was inspired by recommendations for ALMA [48].

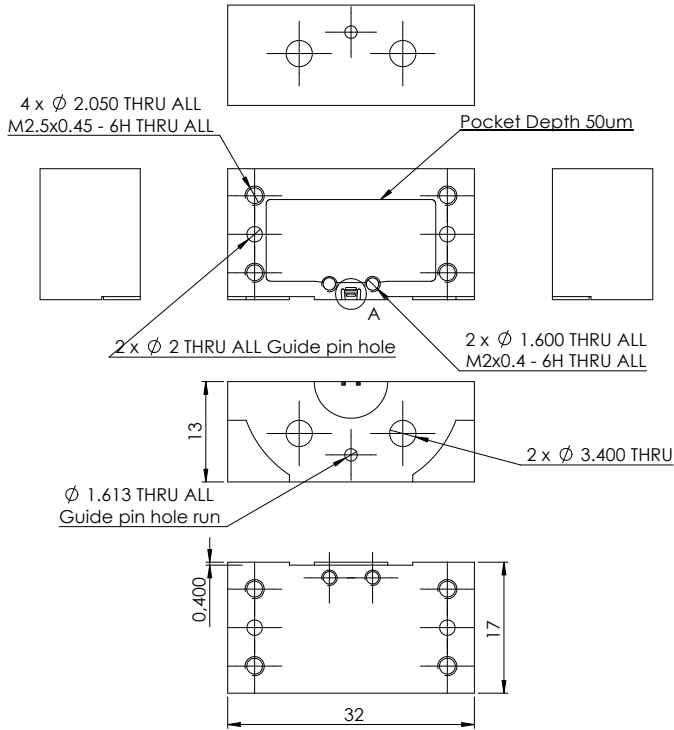


**Figure 4.6:** Lower half of DUT waveguide block. (Waveguide dimensions in mm.)

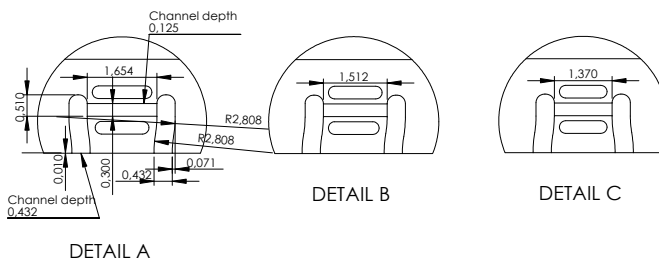


**Figure 4.7:** Detail A: Line 2, Reflect, DUT. Detail B: Line 1, DUT. Detail C: Thru. Waveguide straight sections are parallel, and the bends continue tangentially to the previous section. (Waveguide dimensions in mm.)

## 4.2 Terahertz integrated membrane circuit processing

The membrane circuits were manufactured in an in-house clean room process. The 3  $\mu\text{m}$  thick GaAs membrane is epitaxially grown on an GaAs (100) substrate, with a thin (nm) etch-stop-layer of AlGaAs inbetween, see Figure 4.8a. The etch-stop layer is used on both front- and back side process, for defining the membrane and releasing it from the substrate. Since the layer thickness can be determined with great accuracy in the epitaxial growth process, this ensures an accurate membrane thickness.

The shape of the membrane that the circuit will rest on is defined in a photolithography step and then wet etched, see Figure 4.8b and Figure 4.8c. A wet etch consisting of citric acid and  $\text{H}_2\text{O}_2$  was used to etch away all membrane layer material except the areas protected by the resist. This wet etch is used for its selective etching properties, etching GaAs much faster than  $\text{Al}_x\text{Ga}_{1-x}\text{As}$  [52–54].

The GaAs surface is protected from sputtered gold using a thin layer of SiN. The SiN is grown in a plasma enhanced chemical vapour deposition (PECVD) process with a deposited thickness of 230 nm. Next, a dry etching step in order to open windows in the SiN where the circuit metal will be deposited, was performed.

The edges of the membrane was protected by a thick layer of photoresist, which was patterned and then a reflow process was used to give the layer a soft profile. Next, a seed layer for the electro plating was formed from a thin layer of Ti/Au, deposited by plasma sputtering, see Figure 4.8d. Photolithography was used to pattern the circuit, which was electro plated with a 2  $\mu\text{m}$  layer of gold, see Figure 4.8e. After electro plating, the photoresist was removed, and the metal seed layer between the circuits removed by ion milling, see Figure 4.8f.

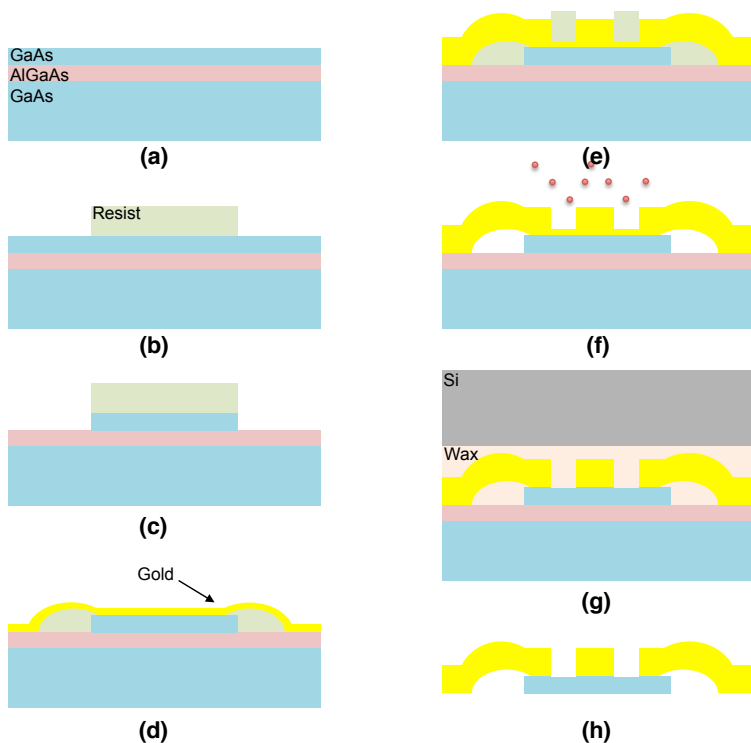


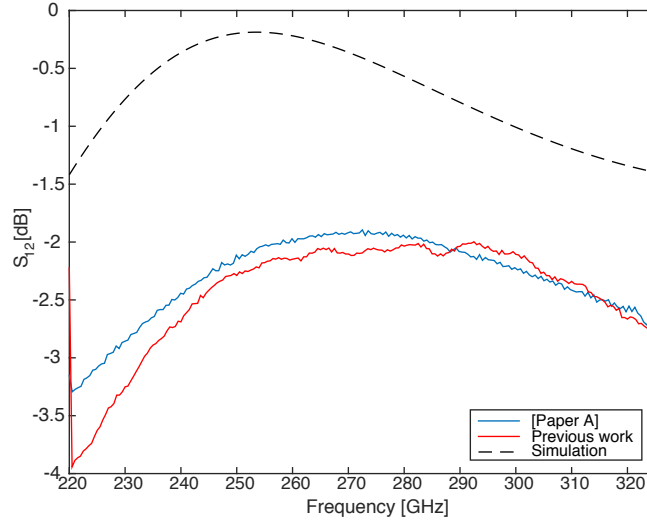
**Figure 4.8:** Cross section of the membrane process in order: (a) GaAs substrate with epitaxial AlGaAs etch stop and GaAs membrane layers. (b) Pattern membrane with photo-resist. (c) Wet-etch membrane layer. (d) Protect membrane edges with photo-resist, reflow resist, deposit Ti/Au seed layer in sputter. (e) Pattern circuit with photo-resist, then deposit gold through electro-plating. (f) Remove resist, then use ion-milling to remove Ti/Au seed layer. (g) Attach Si-wafer on front side with melted wax, then lapp down back side. (h) Wet etch all of the substrate from back, then rinse and release membrane circuits from Si-wafer.

In order to release the membrane circuit from the substrate, the front side was waxed onto a silicon substrate, see Figure 4.8g. The wax protects the front side during the back side processing, and the silicon serves as a carrier substrate after the GaAs substrate has been removed. The GaAs substrate is removed in two steps, first it is thinned down by lapping, then the remaining substrate is removed in a wet etch process. Finally the membrane circuits were released from the Si-carrier and ready for assembly in the waveguide block, see Figure 4.8h.

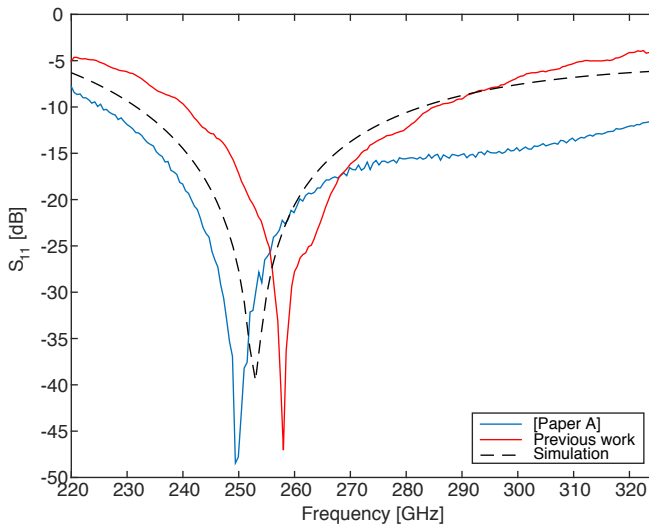
### 4.3 Circuit measurement results

Two different devices were measured, a ring resonator circuit and a shorted stub circuit, and the result was presented in [Paper A]. In Figure 4.9a and Figure 4.9b  $S_{12}$  and  $S_{11}$ , of the double stub structure in the new setup is plotted together with simulation results and measurements of the same structure in the old setup [36]. The ripples in the measurement are visibly reduced.

The higher losses compared to simulation can be due to poor electrical contact between beam leads and waveguide block.



(a)



(b)

**Figure 4.9:**  $S_{21}$  and  $S_{11}$  of shorted stub circuit measurement in [Paper A] compared with the previous work and simulations.



## Chapter 5

# Conclusion and future outlook

The main driver in this thesis has been to reduce the phase uncertainty, due to access waveguide width tolerance of the calibration standard and DUT blocks. A novel single-flange 2-port TRL calibration kit and S-parameter measurement setup with drastically shortened access waveguides was presented, that improved results compared to previous work. The uncertainty was investigated with simulations, however, it is difficult to measure the uncertainty. Instead we rely on measurements on DUTs, and the quality of those measurements, for proof of concept.

The measurements performed using the presented setup and TRL-kit on two different DUTs, a ring resonator circuit, and a shorted stub structure, proved good connection repeatability in both amplitude and phase. The repeatability between the measured sets were between  $0^\circ$  and  $10^\circ$ , which is in the same order as the stability of the frequency extenders, of  $\pm 8^\circ$  [55]. Moreover, the ripples seen in measurements performed with the conventional setup, was eliminated with this setup, and the measured

S-parameters were in agreement with simulation results.

All other things being equal, the introduction of the adapter block also improved uncertainty, by eliminating the cable flex. It also made it easier to reconnect the block, compared to the conventional setup, where it was difficult to reach screws and screw holes, and align the waveguide flanges without gaps. The change time was shortened as well by this, improving phase uncertainty due to VNA drift.

A major drawback with the presented setup, if one wants to measure on different devices, is that the distance between the inputs in the same flange is constant. This means that in order to measure on a longer device, such as a filter structure with multiple impedance sections, one must manufacture a new test set of both adapter, calibration and DUT blocks.

The presented TRL-kit has potential for further development in the future. Future works include scaling the setup up in frequency, and including bias circuitry to analyse active devices, such as Schottky diodes. By adding bias circuitry, active two-terminal devices, such as Schottky diodes, can be characterised. The improved measurement uncertainty will aid in being able to measure and extract an accurate model of the device and its parasitic elements. However, the effect of the bias circuitry on measurement uncertainty need to be investigated.

There is also a need for measurements at higher frequencies, where there may be an advantage to perform waveguide integrated measurements, rather than on-wafer probing. Potential difficulties when moving up in frequency is the scaling of error with the scaling of the dimensions of the access waveguides. Since access waveguide width tolerance is equally large for higher frequencies, the phase error scales as  $T \propto (1/\lambda^2)$  for a constant waveguide length, which means that the access waveguides need to be even shorter at higher frequencies, to provide the same phase uncertainty.

We have shown that by investigating the trade-offs between sources of uncertainty, they can be improved even though another error is introduced. The measurement uncertainty introduced by the waveguide bends was compensated for by the reduction of access waveguide length and the adapter block keeping the VNA extender cables locked in position. The setup enables measurements with drastically improved uncertainty, which will be necessary for characterising active THz integrated membrane devices, such as Schottky diodes at THz frequencies.



## Chapter 6

# Summary of appended papers

### Paper A

#### **Single-flange 2-port TRL calibration for accurate THz S-parameter measurements of waveguide integrated circuits**

In this paper a new setup for S-parameter measurements on passive waveguide integrated membrane circuit components, using TRL calibration is described and tested at 220-325 GHz. The setup consists of two waveguide blocks, where the first block take the two inputs from the VNA and put them in the same flange. This block stays fixed during the measurements, also keeping the two VNA extenders locked in position. The second block is interchangeable, containing the calibration circuits and the DUT. Since the in- and output is put in one single flange, the access waveguides can be very short. This, together with the block locking the VNA in position, improves the measurement uncertainty

due to extender cable flex and waveguide block manufacturing tolerances greatly.

**My contribution:** Writing the paper, main idea, waveguide block designs, membrane circuit manufacturing and circuit mounting, measurements. Calibration and analysis was performed in close collaboration with Dr. J. Stenarson and Dr. K. Yhland.

## Paper B

### Single flange 2-port design for THz integrated circuit S-parameter characterization

This paper focus on the design of the above setup. In particular on the trade-off between measurement uncertainty caused by longer access waveguides compared to shorter bend radius, for different introduced waveguide width errors. It was found that the phase uncertainty is within  $-8^\circ$  to  $12^\circ$  for a bend radius  $r = 6w_y$ , and a  $\pm 10 \mu\text{m}$  width tolerance.

**My contribution:** Writing the paper, main idea (in collaboration with Dr. P. Sobis and Dr. T. Bryllert), 3D EM FEM model and simulations.

# Acknowledgements

This work would not have been possible without the collaboration with, and help and support from others. For this, I am grateful.

To my supervisor, Prof. Jan Stake, and co-supervisor Adj. Prof. Klas Yhland, thank you for all your support, guidance and encouragement. I would also like to thank Dr. Jörgen Stenarson, for a great collaboration, and also for patiently taking his time to answer all my questions.

Thank you Dr. Tomas Bryllert and Dr. Peter Sobis, my informal supervisors, without whom there wouldn't have been a single flange 2-port TRL kit. Never underestimate the power of just having a cup of coffee together!

To my co-supervisor, Dr. Huan Zhao, and to Vladimir Drakinskiy and Dr. Josip Vukusic, thank you for your guidance and sharing of your knowledge in the clean room, and to the Nanofabrication Laboratory staff. And Carl-Magnus Kihlman, for being so helpful when machining the waveguide blocks, Dr. Klas Eriksson for setting up the measurement equipment, and Dr. Aik Yean Tang for sharing of measurement scripts.

I want to thank Robin Dahlbäck and Arvid Hammar, and friends and colleagues in the Terahertz and Millimetre Wave Laboratory, and the Gigahertz Centre, for creating a fun and friendly atmosphere at work.

Finally I would like to thank my husband, Andreas Hanning,

for his love and support.

This research has been carried out in the Gigahertz Centre in a joint research project financed by the Swedish Governmental Agency for Innovation Systems (VINNOVA), Chalmers University of Technology, Omnisys Instruments AB, Wasa Millimeter Wave AB, Low-Noise Factory and SP Technical Research Institute of Sweden.

*Johanna Hanning*

*Göteborg  
May 15, 2015*

# References

- [1] P. H. Siegel, “Terahertz technology,” *IEEE Transactions on Microwave Theory and Techniques*, vol. 50, no. 3, pp. 910–928, 2002.
- [2] —, “THz Instruments for Space,” *IEEE Transactions on Antennas and Propagation*, vol. 55, no. 11, pp. 2957–2965, Nov. 2007.
- [3] J. C. Wiltse, “History of Millimeter and Submillimeter Waves,” *IEEE Transactions on Microwave Theory and Techniques*, vol. 32, no. 9, pp. 1118–1127, 1984.
- [4] J. S. Santos. (2014, Dec.) Herschel’s view of the early Universe reveals galaxy cluster fireworks. [Online]. Available: <http://sci.esa.int/herschel/55150-herschel-view-of-the-early-universe-reveals-galaxy-cluster-fireworks/>
- [5] (2013, Mar.) Juice. [Online]. Available: <http://sci.esa.int/juice/50073-science-payload/>
- [6] M. Tonouchi, “Cutting-edge terahertz technology,” *Nature Photonics*, vol. 1, no. 2, pp. 97–105, Feb. 2007.
- [7] Z. Popovic and E. N. Grossman, “THz Metrology and Instrumentation,” *IEEE Transactions on Terahertz Science and Technology*, vol. 1, no. 1, pp. 133–144, 2011.

- [8] N. Ginsburg, "History of far-infrared research. II. The grating era, 1925–1960," *JOSA*, vol. 67, no. 7, pp. 865–871, Jul. 1977.
- [9] M. J. E. Golay, "A Pneumatic Infra-Red Detector," *Review of Scientific Instruments*, vol. 18, no. 5, pp. 357–362, May 1947.
- [10] N. Erickson, "A Fast, Very Sensitive Calorimetric Power Meter for Millimeter to Submillimeter Wavelengths," in *th International Symposium on Space Terahertz Technology, Harvard University, March, 2002*.
- [11] P. U. Jepsen, D. G. Cooke, and M. Koch, "Terahertz spectroscopy and imaging—Modern techniques and applications," *Laser & Photonics Reviews*, 2011.
- [12] P. Goy and M. Gross, "Millimeter and/or submillimeter network vector analyzer," Patent US005 119 035A, Jun., 1992.
- [13] P. H. Siegel, "Terahertz Pioneer: Philippe Goy "If You Agree With the Majority, You Might be Wrong"," *IEEE Transactions on Terahertz Science and Technology*, vol. 3, no. 4, pp. 348–353, 2013.
- [14] Vector network analyzer extension modules. [Online]. Available: <http://vadiodes.com/index.php/en/products/vector-network-analyzer>
- [15] A. Y. Tang, V. Drakinskiy, K. Yhland, J. Stenarson, T. Bryllert, and J. Stake, "Analytical Extraction of a Schottky Diode Model From Broadband S-Parameters," *IEEE Transactions on Microwave Theory and Techniques*, vol. 61, no. 5, pp. 1870–1878, 2013.
- [16] A. Y. Tang and J. Stake, "Impact of Eddy Currents and Crowding Effects on High-Frequency Losses in Planar

- Schottky Diodes,” *Electron Devices, IEEE Transactions on*, vol. 58, no. 10, pp. 3260–3269, 2011.
- [17] P. H. Siegel, R. P. Smith, M. C. Graidis, and S. Martin, “2.5-THz GaAs monolithic membrane-diode mixer,” *IEEE Transactions on Microwave Theory and Techniques*, vol. 47, no. 5, pp. 596–604, May 1999.
- [18] H. Zhao, V. Drakinskiy, P. J. Sobis, J. Hanning, T. Bryllert, A. Y. Tang, and J. Stake, “Development of a 557 GHz GaAs monolithic membrane-diode mixer,” in *24th International Conference on Indium Phosphide and Related Materials (IPRM)*. IEEE, 2012, pp. 102–105.
- [19] R. A. Pucel, “Design Considerations for Monolithic Microwave Circuits,” *IEEE Transactions on Microwave Theory and Techniques*, vol. 29, no. 6, pp. 513–534, Jun. 1981.
- [20] S. A. Schelkunoff, “Impedance concept in waveguides,” *Quarterly of applied mathematics*, vol. 2, no. 1, Apr. 1944.
- [21] R. B. Marks and D. F. Williams, “A general waveguide circuit theory,” *Journal of Research-National Institute of ...*, vol. 97, no. 5, pp. 533–562, 1992.
- [22] K. Kurokawa, “Power Waves and the Scattering Matrix,” *IEEE Transactions on Microwave Theory and Techniques*, vol. 13, no. 2, pp. 194–202, 1965.
- [23] D. A. Frickey, “Conversions between S, Z, Y, H, ABCD, and T parameters which are valid for complex source and load impedances,” *IEEE Transactions on Microwave Theory and Techniques*, vol. 42, no. 2, pp. 205–211, 1994.
- [24] C. A. Hoer, “The Six-Port Coupler: A New Approach to Measuring Voltage, Current, Power, Impedance, and Phase,”

- IEEE Transactions on Instrumentation and Measurement*, vol. 21, no. 4, pp. 466–470, 1972.
- [25] G. F. Engen, “The Six-Port Reflectometer: An Alternative Network Analyzer,” *IEEE Transactions on Microwave Theory and Techniques*, vol. 25, no. 12, pp. 1075–1080, 1977.
- [26] D. Grischkowsky, S. Keiding, M. van Exter, and C. Fattinger, “Far-infrared time-domain spectroscopy with terahertz beams of dielectrics and semiconductors,” *Journal of the Optical Society of America B*, vol. 7, no. 10, pp. 2006–2015, Oct. 1990.
- [27] R. F. Bauer and P. J. Penfield, “De-Embedding and Unterminating,” *IEEE Transactions on Microwave Theory and Techniques*, vol. 22, no. 3, pp. 282–288, Mar. 1974.
- [28] H. Xu, G. S. Schoenthal, L. Liu, Q. Xiao, J. L. Hesler, and R. M. Weikle II, “On Estimating and Canceling Parasitic Capacitance in Submillimeter-Wave Planar Schottky Diodes,” *IEEE Microwave And Wireless Components Letters*, vol. 19, no. 12, pp. 807–809, Dec. 2009.
- [29] K. Yau, E. Dacquay, I. Sarkas, and S. Voinigescu, “Device and IC Characterization Above 100 GHz,” *IEEE Microwave Magazine*, vol. 13, no. 1, pp. 30–54, Jan. 2012.
- [30] T. J. Reck, L. Chen, C. Zhang, A. Arsenovic, C. Groppi, A. Lichtenberger, R. M. Weikle II, and N. S. Barker, “Micromachined Probes for Submillimeter-Wave On-Wafer Measurements—Part II: RF Design and Characterization,” *IEEE Transactions on Terahertz Science and Technology*, vol. 1, no. 2, pp. 357–363.
- [31] A. Fung, L. Samoska, D. Pukala, D. Dawson, P. Kangaslahti, M. Varonen, T. Gaier, C. Lawrence, G. Boll, R. Lai, and X. B.

- Mei, "On-Wafer S-Parameter Measurements in the 325–508 GHz Band," *IEEE Transactions on Terahertz Science and Technology*, vol. 2, no. 2, pp. 186–192, 2012.
- [32] N. Alijabbari, M. F. Bauwens, and R. M. Weikle, "Design and Characterization of Integrated Submillimeter-Wave Quasi-Vertical Schottky Diodes," *IEEE Transactions on Terahertz Science and Technology*, vol. 5, no. 1, pp. 73–80, 2015.
- [33] H. Zhao, A. Y. Tang, P. J. Sobis, T. Bryllert, K. Yhland, J. Stenarson, and J. Stake, "Submillimeter Wave S-Parameter Characterization of Integrated Membrane Circuits," *IEEE Microwave and Wireless Components Letters*, vol. 21, no. 2, pp. 110–112, 2011.
- [34] —, "VNA-calibration and S-parameter characterization of submillimeter wave integrated membrane circuits," in *Infrared Millimeter and Terahertz Waves (IRMMW-THz), 2010 35th International Conference on*, 2010, pp. 1–2.
- [35] J. Stenarson, K. Yhland, T. N. T. Do, H. Zhao, P. J. Sobis, and J. Stake, "Influence of waveguide width errors on TRL and LRL calibrations," in *79th ARFTG Microwave Measurement Conference*. IEEE, 2012, pp. 1–3.
- [36] J. Stenarson, T. N. T. Do, H. Zhao, P. J. Sobis, A. Y. Tang, K. Yhland, and J. Stake, "Sensitivity Analysis of TRL Calibration in Waveguide Integrated Membrane Circuits," *IEEE Transactions on Terahertz Science and Technology*, vol. 3, no. 5, pp. 558–565, 2013.
- [37] G. F. Engen and C. A. Hoer, "Thru-Reflect-Line: An Improved Technique for Calibrating the Dual Six-Port Automatic Network Analyzer," *IEEE Transactions on Microwave Theory and Techniques*, vol. 27, no. 12, pp. 987–993, 1979.

- [38] D. F. Williams, “500 GHz–750 GHz Rectangular-Waveguide Vector-Network-Analyzer Calibrations,” *IEEE Transactions on Terahertz Science and Technology*, vol. 1, no. 2, pp. 364–377, Nov. 2011.
- [39] W. Kruppa and K. F. Sodomsky, “An Explicit Solution for the Scattering Parameters of a Linear Two-Port Measured with an Imperfect Test Set (Correspondence),” *IEEE Transactions on Microwave Theory and Techniques*, vol. 19, no. 1, pp. 122–123, 1971.
- [40] J. Stenarson and K. Yhland, “A Reformulation and Stability Study of TRL and LRM Using *S*-Parameters,” *Microwave Theory and Techniques*, 2009.
- [41] R. B. Marks, “A multiline method of network analyzer calibration,” *IEEE Transactions on Microwave Theory and Techniques*, vol. 39, no. 7, pp. 1205–1215, Jul. 1991.
- [42] D. F. Williams, J. C. M. Wang, and U. Arz, “An optimal vector-network-analyzer calibration algorithm,” *IEEE Transactions on Microwave Theory and Techniques*, vol. 51, no. 12, pp. 2391–2401, 2003.
- [43] J. Stenarson and K. Yhland, “Residual error models for the SOLT and SOLR VNA calibration algorithms,” in *69th ARFTG Microwave Measurement Conference, 2007*. IEEE, 2007, pp. 1–7.
- [44] —, “Uncertainty Propagation Through Network Parameter Conversions,” *IEEE Transactions on Instrumentation and Measurement*, vol. 58, no. 4, pp. 1152–1157, 2009.
- [45] U. Stumper, “Uncertainty of VNA *S*-parameter measurement due to nonideal TRL calibration items,” *IEEE Transactions*

- on Instrumentation and Measurement*, vol. 54, no. 2, pp. 676–679, 2005.
- [46] H. Li, A. Arsenovic, J. L. Hesler, A. R. Kerr, and R. M. Weikle, “Repeatability and Mismatch of Waveguide Flanges in the 500-750 GHz Band,” *IEEE Transactions on Terahertz Science and Technology*, vol. 4, no. 1, pp. 39–48, Jan. 2014.
- [47] N. M. Ridler and R. G. Clarke, “Investigating connection repeatability of waveguide devices at frequencies from 750 GHz to 1.1 THz,” in *82nd ARFTG Microwave Measurement Conference*. IEEE, 2013, pp. 1–13.
- [48] A. R. Kerr, E. Wollack, and N. Horner. (1999, Nov.) Waveguide Flanges for ALMA Instrumentation. [Online]. Available: <http://library.nrao.edu/public/memos/alma/memo278.pdf>
- [49] F. Mubarak, G. Rietveld, D. Hoogenboom, and M. Spirito, “Characterizing cable flexure effects in S-parameter measurements,” in *82nd ARFTG Microwave Measurement Conference*. IEEE, 2013, pp. 1–7.
- [50] J. C. Liu and K. Wong, “Test port cable instability and VNA measurement errors,” in *2013 81st ARFTG Microwave Measurement Conference (ARFTG)*. IEEE, Aug. 2013.
- [51] N. M. Ridler, “Choosing Line Lengths for Calibrating Waveguide Vector Network Analysers at Millimetre and Sub-millimetre Wavelengths,” National Physics Laboratory, Teddington, Middlesex, United Kingdom, Tech. Rep. NPL Report TQE 5, Mar. 2009.
- [52] E.-A. Moon, J.-L. Lee, and H. M. Yoo, “Selective wet etching of GaAs on  $\text{Al}_x\text{Ga}_{1-x}\text{As}$  for AlGaAs/InGaAs/AlGaAs

- pseudomorphic high electron mobility transistor,” *Journal Of Applied Physics*, vol. 84, no. 7, pp. 3933–3938, 1998.
- [53] J.-H. Kim, D. H. Lim, and G. M. Yang, “Selective etching of AlGaAs/GaAs structures using the solutions of citric acid/H<sub>2</sub>O<sub>2</sub> and de-ionized H<sub>2</sub>O/buffered oxide etch,” *Journal of Vacuum Science & Technology B: Microelectronics and Nanometer Structures*, vol. 16, no. 2, pp. 558–560, 1998.
- [54] H. J. Lee, M. S. Tse, K. Radhakrishnan, K. Prasad, J. Weng, S. F. Yoon, X. Zhou, H. S. Tan, S. K. Ting, and Y. C. Leong, “Selective wet etching of a GaAsAl<sub>x</sub>Ga<sub>1-x</sub>As heterostructure with citric acid-hydrogen peroxide solutions for pseudomorphic GaAs/Al<sub>x</sub>Ga<sub>1-x</sub>As/In<sub>y</sub>Ga<sub>1-y</sub>As heterojunction field effect transistor fabrication,” *Materials Science and Engineering: B*, vol. 35, no. 1, pp. 230–233, 1995.
- [55] OML Inc. (2012, Jun.) V03VNA2 Series WR03 Frequency Extension Modules 220 to 325 GHz. [Online]. Available: [http://www.omlinc.com/images/pdf/VxxVNA2/OML-V03VNA2\\_Datasheet.pdf](http://www.omlinc.com/images/pdf/VxxVNA2/OML-V03VNA2_Datasheet.pdf)